RESEAPRO
JOURNALS

ORIGINAL ARTICLE

OPEN ACCESS

Thermo-mechanical characterization of plasma sprayed YSZ-CeO² nanocomposite coatings

Sashikanta Sethi[1,2], Sisir Mantry[1,2], Spandan Patra[3], Sandip Kumar Nayak[4], Sambit K Parida[5] and Laxmidhar Besra[1,2]

[1]Department of Materials Chemistry, CSIR-Institute of Minerals and Materials Technology, Bhubaneswar, India
[2]Academy of Scientific and Innovative Research (AcSIR), Uttar Pradesh, India
[3]Department of Mechanical Engineering, National Institute of Technology, Rourkela, India
[4]Department of Mechanical Engineering, Indian Institute of Technology Delhi, New Delhi, India
[5]Department of Mechanical & Manufacturing Engineering, National Institute of Advanced Manufacturing Technology (NIAMT), Jharkhand, India

ABSTRACT

The optimization of process parameters was essential when creating YSZ-CeO$_2$ nanocomposite coatings using atmospheric plasma spraying. Using particle diagnostics, the molten state of nano agglomerates was carefully observed to maintain their nanostructure, including temperature and velocity. The research focused on the microstructure, thermal diffusivity, and adhesion strength of the nanocomposite coatings applied through spraying. FESEM examination uncovered a dual-phase microstructure, with nano-regions embedded in a fully molten particle matrix. The dual structure caused a decrease in the thermal conductivity of nano YSZ coatings, due to phonon scattering at grain boundaries, point defect scattering, and higher inter-splat porosity in comparison to bulk coatings. The addition of CeO$_2$ played a major role in causing this decrease. XRD analysis verified that tetragonal zirconia was present, and the average grain size of as-sprayed CeYSZ coatings varied from 90 to 120 nm. The improved thermal and mechanical characteristics were mainly a result of increased interfacial toughness, which was brought about by the existence of adherent nano regions and the dense coating structure. This research showcases the capabilities of YSZ-CeO$_2$ nanocomposite coatings for use in situations where high thermal and mechanical performance is needed.

Introduction

Thermal barrier coatings (TBCs) are vital for enhancing the efficiency and longevity of high-temperature components in gas turbines and diesel engines [1-6]. Among various materials, yttria-stabilized zirconia (YSZ) has emerged as the primary choice for TBCs due to its favourable properties, which include low thermal conductivity, phase stability at elevated temperatures, high coefficient of thermal expansion (CTE), and chemical inertness in harsh environments [7-11]. However, YSZ is susceptible to phase changes at temperatures exceeding 1200°C, leading to coating degradation and reduced service life [9].

To overcome these limitations, researchers have explored the incorporation of cerium oxide (CeO$_2$) into YSZ coatings. The integration of CeO$_2$ has shown promise in enhancing the corrosion resistance, fracture toughness, and thermal insulation capabilities of the coatings [9]. Furthermore, the development of nanostructured zirconia materials, characterized by grain sizes smaller than 100 nm, has been demonstrated to improve mechanical properties such as increased hardness, yield strength, and wear resistance [12]. Compared to traditional micro-structured coatings, nanostructured zirconia coatings fabricated through thermal spray techniques offer unique advantages, including lower thermal conductivity, greater toughness, and a higher CTE (As Figure 1 shows) These properties make them suitable for applications that require exceptional thermal and mechanical performance under

extreme conditions [13,14]. Nonetheless, maintaining the nanoscale structure during the spraying process remains a challenge, as grain coarsening can occur, compromising phase stability.
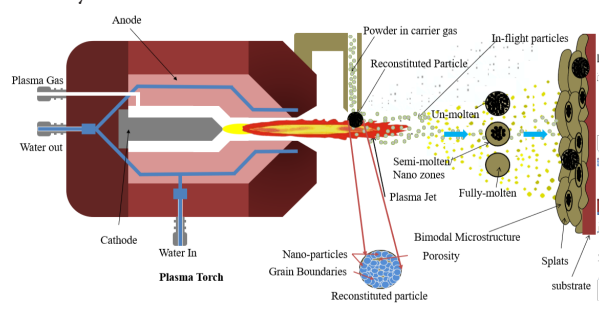

Figure 1. Re-modelling SWCNT's schematic under traverse loading on a foundation.

Recent investigations have focused on doping YSZ with elements such as lanthanum oxide (La$_2$O$_3$) and cerium oxide (CeO$_2$) to further enhance its properties. These dopants have been found to not only decrease thermal conductivity but also improve sintering resistance, thus extending the operational limits of TBCs [15,16]. Composite coatings, such as those combining Y$_2$O$_3$, ZrO$_2$, and CeO$_2$, have also attracted attention for their superior stability at high temperatures, high

fracture toughness, and enhanced corrosion resistance [17].

The objective of this research article is to examine how nano structuring and the addition of CeO₂ affect the microstructural and thermo-mechanical properties of plasma-sprayed YSZ coatings. Through a comprehensive analysis of existing research and experimental findings, this study aims to provide insights into potential advancements and challenges in the development of advanced thermal barrier coatings for next-generation industrial applications. The incorporation of CeO₂ into YSZ coatings and the development of nanostructured zirconia materials represent promising approaches to enhancing the performance of thermal barrier coatings. The addition of CeO₂ improves the corrosion resistance, fracture toughness, and thermal insulation properties of the coatings, while nano structuring enhances their mechanical properties. Doping YSZ with elements such as La₂O₃ and CeO₂ further improves the thermal and mechanical performance of the coatings, extending their operational limits. Composite coatings combining Y₂O₃, ZrO₂, and CeO₂ offer superior stability, toughness, and corrosion resistance, making them suitable for demanding industrial applications.

Experimental

Synthesis of nanostructured powders by sol-gel route

The researchers in this study created nanostructured yttria-stabilized zirconia (YSZ) powders using the sol-gel method, which is recognized for its ability to produce consistent and small-grained ceramic materials [18]. Dissolving zirconium oxychloride and yttrium oxide precursors in a water-based solution with stoichiometric proportions yielded 8 mol% YSZ. After the addition of nitric acid for pH adjustment and homogeneity, the mixture was subjected to constant stirring and heating at 100-120°C. The solution, which included a small quantity of citric acid, was then heated on a hot plate approximately (200-250°C) until it turned into a thick black gel. The gel was burned to create black ashes, which were then processed at 350°C in air to get rid of volatile materials and heated at 600°C to remove carbon impurities, resulting in pure YSZ powder.

In the Figure 2, transmission electron micrograph shows the YSZ powders made through synthesis in displaying an average grain size of 80 to 90 nm, typical of nanostructured materials created using the sol-gel method. In the experimental arrangement, the YSZ powder was combined with nano CeO₂ particles ranging in size from 10 to 30 nanometers (Product Code 2110 CG) sourced from Sky Spring Nanomaterials, Inc., USA.
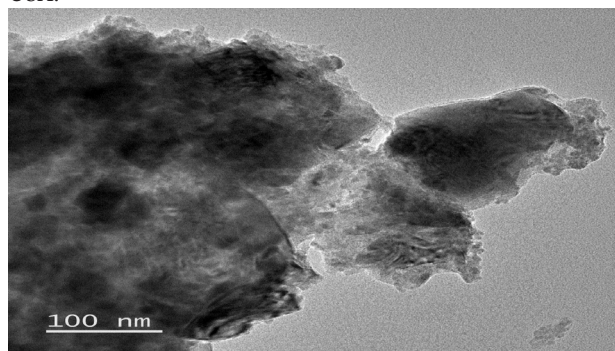
Both YSZ and CeO₂ powders underwent heat treatment at 1400°C to ensure homogeneity and phase stability prior to plasma spraying. This high-temperature treatment is crucial for consolidating the powders and enhancing their suitability for thermal barrier coating applications, where stability and durability under extreme operating conditions are paramount.

Reconstitution of nanopowders

A nano-scale powder composed of 10CeYSZ, with 90%wt YSZ (5.4% Y2O₃-ZrO₂) and (10% CeO₂), was made for plasma coating Inconel 718 surfaces [19]. The first nano CeYSZ powder, containing evenly spread-out nanoparticles, was clumped together to reach particle sizes suitable for plasma spraying, varying from around 30 to 90 μm. The spray-drying technique in a Buchi B-290 research model spray dryer facilitated the agglomeration process.

During the production of the spray-drying suspension, nano CeO₂ and nano YSZ powders were combined with a 2 wt.% polyethylene glycol (PEG) binder and 1 wt.% ammonium citrate. The suspension was subjected to intense ball-milling for more than 24 hours in order to guarantee equal dispersion. After that, they used intense magnetic stirring and heating up to 300K in order to create a uniform nano-CeYSZ slurry. The inclusion of a PEG binder was essential for bonding the nanoparticles via Van der Waals forces, aiding in the creation of spherical droplets during atomization.

The spray-dried granules were gathered and sifted to create round agglomerates of around ~50 μm in diameter. The agglomerates continued to have nanoscale grain sizes between 80 and 90 nm, as shown in Figure 3a. Analysis of the powder mixture after spray drying using X-ray diffraction confirmed the existence of tetragonal zirconia and cubic ceria phases, as depicted in Figure 3b.
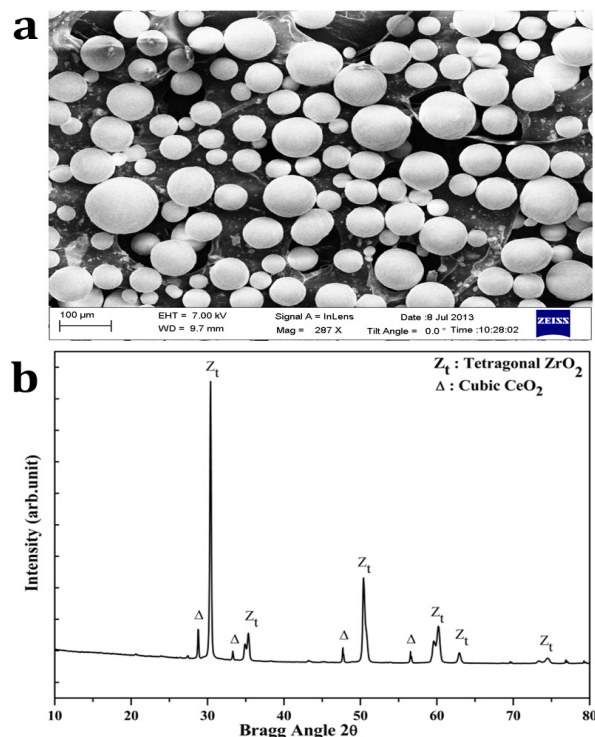
Figure 3. FESEM & XRD of spray-dried CeYSZ particles.

Figure 2. TEM micrograph of as-synthesized YSZ particles.

J. Coat. Technol. Innov., 2024, 2, 19-24

20

Development of coatings

In order to improve adhesion between surfaces, the substrate was subjected to grit blasting, which involved using highly compressed air to spray alumina particles and create a uniform roughness of 6-8 μm. The application was carried out in CSIR-IMMT, Bhubaneswar, using an 80-kW plasma spray system from Metallization, U.K. Pure argon was the main plasmagen gas, while helium was the secondary gas at a 4 kg/cm² outlet pressure. A substrate of Inconel 718, with dimensions of 120×60×5 mm³, was prepared with grit blasting before being placed on a turntable for the application of CeYSZ nanocomposite powders, with process parameters adjusted according to Table 1.

Table 1. Selected operating parameters for the plasma spray coating process (Top Coat).

Parameter	Operating Range
Operating Power	38 kW
Current	865 amps
Primary Plasmagen gas (Argon) flow rate	40 lpm
Secondary Plasmagen gas (Hydrogen) Flow rate	0.5 lpm
Carrier Gas flow rate	5 lpm
Nozzle to substrate distance (Stand-off distance)	80 mm
Powder feed rate	25 g/ min

Before the CeYSZ coating was applied, NiCrCoAlY bond coats about 100 μm in thickness were applied to the substrates using HVOF (Hipojet 2700, m/s MEC, Jodhpur, India). Table 2 outlines the deposition process parameters for the bond coats, keeping layer thicknesses consistent to achieve a thickness of around 250 μm for all coatings, including the bond coat.

Table 2. Selected operating parameters for the HVOF process (Bond Coat).

Parameter	Operating Range
Oxygen Pressure	10 bar
Oxygen Flow rate	265 lpm
LPG Pressure	7 bar
LPG flow rate	70 lpm
Air pressure	5 bar
Air flow rate	700 lpm
Carrier gas (Nitrogen) Pressure	6 bar
Carrier gas flow rate	6.5 lpm
Air Cap	9.3 mm

Characterizations

The X-ray diffractometer (Rigaku Ultima IV) with CuKα radiation and a Ni filter was used to examine the crystal structure of the synthesized nanocomposite powders and coatings. Tests were carried out at ambient temperature across a 2-theta spectrum from 20 to 80 degrees in order to determine the phases found in the calcined powder. (FESEM: Zeiss SupraTM55) was used to analyze the microstructure and measure the average grain size of the coatings.

Measurements of thermal diffusivity were conducted at different temperatures using the laser flash technique (LFA 1000, LINSEIS). Parker et al. [20] initially suggested this method of heating samples from ambient temperature to the target temperature and taking three measurements at each temperature. The mean of these values was stated. In order to guarantee precise measurements, a thin carbon film was added to the specimen surfaces to improve laser pulse absorption.

$$\text{Thermal diffusivity, } \alpha = 0.1388 \frac{L}{t_{/2}} \tag{1}$$

The thermal conductivity of each sample was determined using the given equation, which incorporates the sample's thickness (cm) and t1/2, the time taken for the rear surface to reach half of the maximum temperature rise (s).

$$\text{Thermal conductivity, } k(T) = \alpha(T) . \rho . C\_p(T) \tag{2}$$

Archimedes principle, and specific heat (Cp(T)) measured with a differential scanning calorimeter.

The adhesion of the coatings was tested using the pull-out method specified in Figure 4 as per ASTM C633 standard. The measuring of coating adhesion through tensile strength involved dividing the maximum load at rupture at the coating-substrate interface by the cross-sectional area of the cylindrical specimen.

Figure 4. Plasma spraying torch and adhesion test set-up as per ASTM C-633 standard.

Online particle diagnostics

The properties of thermal barrier coatings are intricately linked to the characteristics of their constituent lamellae, which are profoundly influenced by the conditions under which particles travel and the substrate temperature during spraying. Microstructural features play a pivotal role in determining coating performance and properties, governed by both particle state and deposition conditions. During spraying, real-time diagnostics using Spray Watch 2i equipment were utilized to evaluate particle velocity and temperature under different conditions, as shown in Figure 5a and 5b. The camera-to-spray gun distance, which was equal to the stand-off distance used during coating application (150 and 200 mm), was kept constant. Particle temperature was determined using two-color pyrometry, and in-flight velocities were calculated by measuring the length of particle traces captured by a high-speed CCD camera during known exposure times [21]. Findings showed a particle temperature around 2650 ± 50°C and speeds close to 200 ± 50 m/sec before hitting, slightly below YSZ's melting point of about 2700°C [13].

Figure 5. Particle velocity and temperature profile by CCD camera.

Results and discussions

Structural Analysis

Figure 6 shows X-ray diffraction (XRD) patterns of bulk yttria-stabilized zirconia (YSZ), nanocrystalline YSZ, and CeYSZ nanocomposite coatings for comparison. These patterns point out the structural variances seen in the coatings in comparison to the standard polycrystalline YSZ coatings that are commonly used as a reference. The X-ray diffraction examination of nanocrystalline YSZ coatings produced through chemical processes shows a cubic zirconia arrangement, with little sign of Y_2O_3 impurity phases. Significantly, the intensity of the peak at (111) is increased and moves to smaller 2θ values, suggesting the presence of strain in the nanostructured YSZ coating. On the other hand, nanocrystalline CeYSZ composite powders show stronger peaks related to tetragonal YSZ phases and cubic CeO_2. After applying the coating, XRD patterns clearly display tetragonal zirconia phases matching JCPDS File no. 30-1468, with no noticeable Y_2O_3 peaks present.
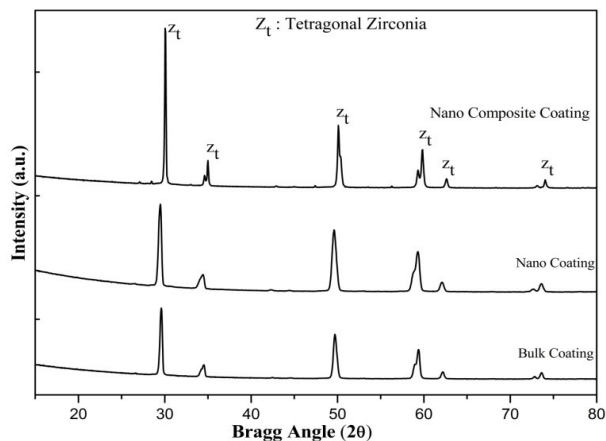

Figure 6. XRD patterns of bulk polycrystalline YSZ coating, nanostructured YSZ coating and CeYSZ nanocomposite coating.

Crucially, the absence of peaks corresponding to monoclinic zirconia and CeO_2 clusters in the nanocomposite coatings indicates that CeO_2 is uniformly dissolved within the ZrO_2 matrix, enhancing phase stability and performance.

Surface morphology analysis

Figure 7, displays field emission scanning electron micrographs illustrating the microstructure of the coatings. In Figure 7a, the fractured cross-section reveals a bimodal microstructure characterized by regions of dense and smooth morphology, indicative of well-molten particles, alongside rough and porous areas suggesting partially molten or unmolten particles. The presence of nano-zones and micro-cracks enhances phonon

scattering, thereby contributing to the reduction in thermal diffusivity. More detailed images Figure 7b shows a surface that is filled with tiny grains closely packed together, with an average grain size ranging from 90 to 120 nanometers. The micrographs exhibit densely packed grains with clearly defined boundaries, lacking voids or porous structures.
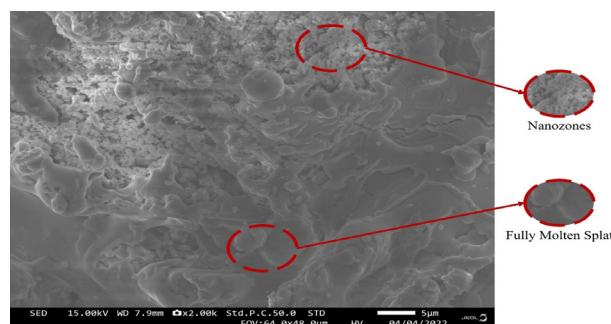

Figure 7. FESEM micrographs of YSZ-CeO₂ nanocomposite coatings.

In Figure 8, energy dispersive X-ray spectroscopy (EDXS) spectra confirm the presence of cerium (Ce) as a dopant in the coating. This doping contributes to lowering the thermal conductivity of the coating, enhancing its thermal insulation properties.
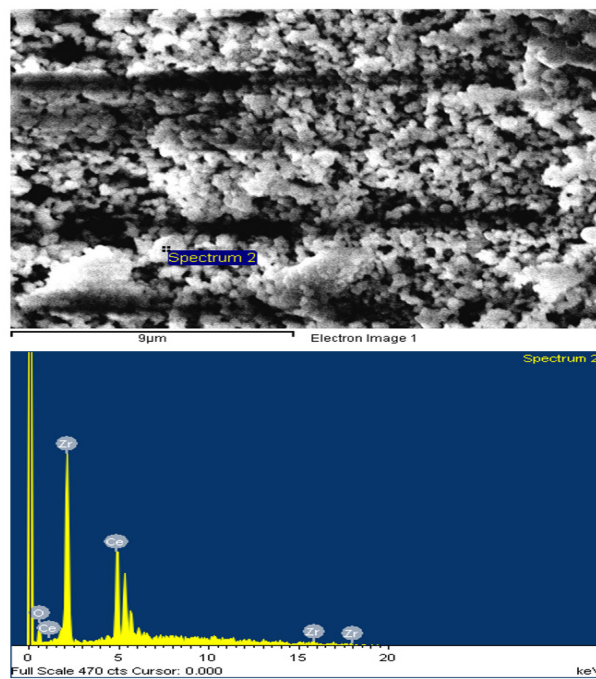

Figure 8. Energy dispersive X-ray spectrum of plasma sprayed YSZ-CeO₂ nanocomposite coating on the marked area.

Adhesion test results

Adhesion testing was conducted on substrates coated with APS, using Taguchi's L16 orthogonal design, which showed that nano YSZ coatings achieved a peak adhesion strength of 40.56 MPa [22]. In the same way, CeYSZ nanocomposite coatings were tested with optimal process parameters, showing different adhesion strengths at various torch input powers, as shown in Figure 9. The adhesion strength of CeYSZ variants showed a slight enhancement compared to nano YSZ coatings. The improvement is credited to the dense and consistent microstructure of the coatings when sprayed, as well as the creation of Ce-diffusion layers in the splats, which strengthen the adhesive forces between them.   Mantry et al. also noted similar improvements in coating adhesion when copper slag was used to dope alumina [23]. The nano CeYSZ nanocomposite reached a peak adhesion strength of 42.39 MPa with a torch input power of 40 kW.
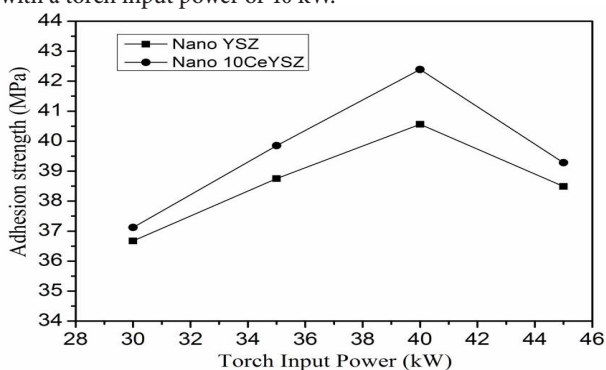

Figure 9. Variation in adhesion strength with input power of as-sprayed nano YSZ coatings [23] and CeYSZ nanocomposite coatings.

Thermal characterization

Figure 10, shows the differences in thermal diffusivity values from room temperature to 1200°C for bulk YSZ, nano YSZ, and 10CeYSZ coatings. The thermal diffusivity of CeO_2-YSZ nanocomposite coatings is consistently lower than that of nano YSZ and bulk YSZ coatings on Inconel 718 substrates. Beginning at 0.3950 x 10^-6 m^2/s at room temperature, the thermal diffusivity reduces to 0.2512 x 10^-6 m^2/s at 900°C, and then slightly rises to 0.2913 x 10^-6 m^2/s at 1200°C [9]. This rise in temperatures is probably caused by increased radiative heat transfer inside the material.
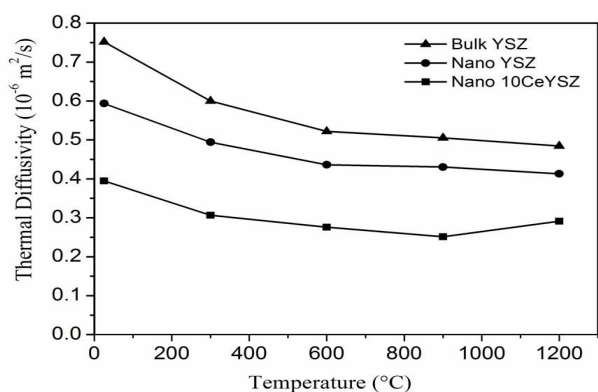

Figure 10. Variation in adhesion strength with input power of as-sprayed nano YSZ coatings [23] and CeYSZ nanocomposite coatings.

A comparable pattern can be seen in the thermal conductivity tests of Figure 11 the covered specimens at different temperature levels. The primary reason for the decrease in thermal diffusivity in nanostructured Thermal Barrier Coatings (TBCs) is mainly due to the smaller grain size of zirconia coatings, which greatly impacts the phonon mean free path as a result of increased grain boundary scattering [24]. Phonon transport mechanisms primarily control heat conduction in zirconia at temperatures lower than 1200°C. Phonons scatter due to interactions with lattice defects like vacancies, grain boundaries, and variations in atomic mass. Additionally, the lower thermal conductivity of nano-coatings can be explained by their higher micro-porosity compared to conventional coatings, which results in increased intersplat gaps [25]. The introduction of dopants like Ce into YSZ introduces significant differences in atomic mass and ionic radius compared to yttrium, thereby enhancing point defect scattering and reducing thermal conductivity [25]. This effect contributes to the overall effectiveness of the Thermal Barrier Coating (TBC) by limiting phonon mean free paths.
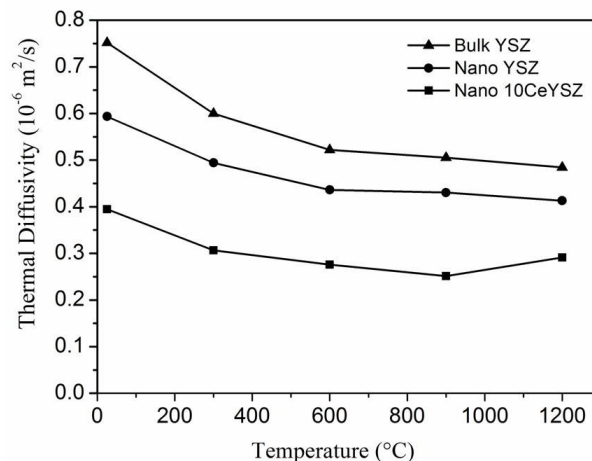

Figure 11. Variation in thermal conductivity with a temperature of as-sprayed conventional YSZ, Nano YSZ, and nanocomposite CeYSZ coatings.

Furthermore, doping-induced strains in the lattice structure due to ionic radius disparities between dopants and host atoms lead to lattice distortions, further scattering atomic vibrational waves between YSZ and the dopant rare earth oxides [25]. Such strain-induced phonon scattering mechanisms have also been observed in plasma-sprayed nanostructured YSZ coatings doped with La_2O_3 [26].

Conclusions

Nanostructured 10CeYSZ coatings created through atmospheric plasma spraying on Inconel 718 surfaces show unique characteristics like melted particles, nano-areas, small cracks, and increased intersplat porosity. Nano CeYSZ coatings exhibit reduced thermal diffusivity in comparison with nano and bulk YSZ coatings, mainly because of phonon scattering at grain boundaries, point defect scattering, and higher intersplat porosity. This mixture of elements improves the thermal insulation characteristics in these coatings.

Examination of the nanocomposite coating's X-ray diffraction (XRD) pattern shows a main cubic phase, as well as

changes in tetragonal and monoclinic phases of YSZ, with some tetragonal phases present. Ce stabilizes ZrO_2 by creating a solid solution, preventing the clustering of Ce in the ZrO_2 matrix in the nanocomposite coating. Surface images show an average grain size that varies from around 90 to 120 nm, displaying densely packed grains connected by tetragonal grain boundary junctions. This specific microstructural organization enhances the durability of the coating and helps in creating Ce-diffusion layers within the splats, which in turn improves adhesion strength.

It is important to monitor the molten state of nano agglomerates through temperature and velocity diagnostics in order to maintain the desired nanostructure. Optimizing process parameters is crucial for achieving and sustaining the intended structural characteristics during the coating process.

Acknowledgment

Disclosure statement

No potential conflict of interest was reported by the authors.

References

1. Gell M. Application opportunities for nanostructured materials and coatings. Mater sci eng. 1995;204(1-2):246-251. https://doi.org/10.1016/0921-5093(95)09969-7

2. Zhu D, Miller RA. Thermal conductivity and elastic modulus evolution of thermal barrier coatings under high heat flux conditions. J Therm Spray Tech. 2000;9:175-180. https://doi.org/10.1361/105996300770349890

3. Padture NP, Gell M, Jordan EH. Thermal barrier coatings for gas-turbine engine applications. Science. 2002;296(5566):280-284. https://doi.org/10.1126/science.1068609

4. Haynes JA, Ferber MK, Porter WD. Thermal cycling behavior of plasma-sprayed thermal barrier coatings with various MCrAlX bond coats. J Therm Spray Tech. 2000;9:38-48. https://doi.org/10.1361/105996300770350041

5. Lucchese P, Jeandin R, Surdon G, Delavernme A. Experimental Approach to Adhesion between an Alumina Plasma-Sprayed Coating and Polymeric Substrate. In International Thermal Spray Conference. ASM International.1996;83805:239-244. https://doi.org/10.31399/asm.cp.itsc1996p0239

6. Tolpygo VK, Clarke DR. The effect of oxidation pre-treatment on the cyclic life of EB-PVD thermal barrier coatings with platinum–aluminide bond coats. Surf Coat Technol. 2005;200(5-6):1276-1281. https://doi.org/10.1016/j.surfcoat.2005.07.088

7. Ni LY, Liu C, Huang H, Zhou CG. Thermal cycling behavior of thermal barrier coatings with HVOF NiCrAlY bond coat. J Therm Spray Tech. 2011;20:1133-1138. https://doi.org/10.1007/s11666-011-9647-8

8. Clarke DR. Materials selection guidelines for low thermal conductivity thermal barrier coatings. Surf Coat Technol. 2003;163:67-74. https://doi.org/10.1016/S0257-8972(02)00593-5

9. Sodeoka S, Suzuki M, Ueno K, Sakuramoto H, Shibata T, Ando M. Thermal and mechanical properties of ZrO_2-CeO_2 plasma-sprayed coatings. J Therm Spray Tech. 1997;6:361-367. https://doi.org/10.1007/s11666-997-0071-z

10. Vasiliev AL, Padture NP. Coatings of metastable ceramics deposited by solution-precursor plasma spray: II. Ternary ZrO_2–Y_2O_3–Al_2O_3 system. Acta Mater. 2006;54(18):4921-4928. https://doi.org/10.1016/j.actamat.2006.06.026

11. Winter MR, Clarke DR. Oxide materials with low thermal conductivity. J Am Ceram Soc. 2007;90(2):533-540. https://doi.org/10.1111/j.1551-2916.2006.01410.x

12. Ibrahim A, Lima RS, Berndt CC, Marple BR. Fatigue and mechanical properties of nanostructured and conventional titania (TiO_2) thermal spray coatings. Surf Coat Int. 2007;201(16-17):7589-7596. https://doi.org/10.1016/j.surfcoat.2007.02.025

13. Lima RS, Marple BR. Thermal spray coatings engineered from nanostructured ceramic agglomerated powders for structural, thermal barrier and biomedical applications: A review. J Therm Spray Tech. 2007;16:40-63. https://doi.org/10.1007/s11666-006-9010-7

14. Wu J, Guo HB, Zhou L, Wang L, Gong SK. Microstructure and thermal properties of plasma sprayed thermal barrier coatings from nanostructured YSZ. J Therm Spray Tech. 2010;19:1186-1194. https://doi.org/10.1007/s11666-010-9535-7

15. Yu Q, Rauf A, Zhou C. Microstructure and thermal properties of nanostructured 4 wt.% Al_2O_3-YSZ coatings produced by atmospheric plasma spraying. J Therm Spray Tech. 2010;19:1294-1300. https://doi.org/10.1007/s11666-010-9524-x

16. Tsipas SA. Effect of dopants on the phase stability of zirconia-based plasma sprayed thermal barrier coatings. J Eur Ceram Soc. 2010;30(1):61-72. https://doi.org/10.1016/j.jeurceramsoc.2009.08.008

17. Zhu D, Chen YL, Miller RA. Defect clustering and nano-phase structure characterization of multi-component rare earth oxide doped zirconia-yttria thermal barrier coatings. In 27th annual cocoa beach conference on advanced ceramics and composites: a: ceramic engineering and science proceedings 2003;525-534. Hoboken, NJ, USA: John Wiley & Sons, Inc. https://doi.org/10.1002/9780470294802.ch75

18. Juarez RE, Lamas DG, Lascalea GE, De Reca NW. Synthesis of nanocrystalline zirconia powders for TZP ceramics by a nitrate–citrate combustion route. J Eur Ceram Soc. 2000;20(2):133-138. https://doi.org/10.1016/S0955-2219(99)00146-6

19. Viswanathan V, Rea KE, Vaidya A, Seal S. Role of spray drying of nanoagglomerates in morphology evolution in nanostructured APS coatings. J Am Ceram Soc. 2008;91(2):379-386. https://doi.org/10.1111/j.1551-2916.2007.02090.x

20. Parker WJ, Jenkins RJ, Butler CP, Abbott GL. Flash method of determining thermal diffusivity, heat capacity, and thermal conductivity. J Appl Phys. 1961;32(9):1679-1684. https://doi.org/10.1063/1.1728417

21. Vattulainen J, Hämäläinen E, Hernberg R, Vuoristo P, Mäntylä T. Novel method for in-flight particle temperature and velocity measurements in plasma spraying using a single CCD camera. J Therm Spray Technol. 2001;10:94-104. https://doi.org/10.1361/105996301770349556

22. Mantry S, Mishra BK, Chakraborty M. Parametric appraisal of process parameters for adhesion of plasma sprayed nanostructured YSZ coatings using taguchi experimental design. Sci World J. 2013(1):527491. https://doi.org/10.1155/2013/527491

23. Mantry S, Behera D, Satapathy A, Jha BB, Mishra BK. Deposition of plasma sprayed copper slag coatings on metal substrates. Surf Eng. 2013;29(3):222-227. https://doi.org/10.1179/1743294412Y.0000000096

24. Soyez G, Eastman JA, Thompson LJ, Bai GR, Baldo PM, McCormick AW, et al. Grain-size-dependent thermal conductivity of nanocrystalline yttria-stabilized zirconia films grown by metal-organic chemical vapor deposition. Appl Phys Lett. 2000;77(8):1155-1157. https://doi.org/10.1063/1.1289803

25. Lehmann H, Pitzer D, Pracht G, Vassen R, Stöver D. Thermal conductivity and thermal expansion coefficients of the lanthanum rare-earth-element zirconate system. J Am Ceram Soc. 2003;86(8):1338-1344. https://doi.org/10.1111/j.1151-2916.2003.tb03473.x

26. Rauf A, Yu Q, Jin L, Zhou C. Microstructure and thermal properties of nanostructured lanthana-doped yttria-stabilized zirconia thermal barrier coatings by air plasma spraying. Scr Mater. 2012;66(2):109-112. https://doi.org/10.1016/j.scriptamat.2011.10.017